

Isometry invariant shape recognition of projectively perturbed point clouds by the mergegram extending 0D persistence

Yury Elkin

Materials Innovation Factory and Computer Science department, University of Liverpool, UK
yura.elkin@gmail.com

Vitaliy Kurlin

Materials Innovation Factory and Computer Science department, University of Liverpool, UK
vitaliy.kurlin@gmail.com

Abstract

Rigid shapes should be naturally compared up to rigid motion or isometry, which preserves all inter-point distances. The same rigid shape can be often represented by noisy point clouds of different sizes. Hence the isometry shape recognition problem requires methods that are independent of a cloud size. This paper studies stable-under-noise isometry invariants for the recognition problem stated in the harder form when given clouds can be related by affine or projective transformations. The first contribution is the stability proof for the invariant mergegram, which completely determines a single-linkage dendrogram in general position. The second contribution is the experimental demonstration that the mergegram outperforms other invariants in recognizing isometry classes of point clouds extracted from perturbed shapes in images.

2012 ACM Subject Classification Theory of computation → Computational geometry

Keywords and phrases Shape Recognition; Topological Data Analysis; Machine Learning; Computer Vision

Digital Object Identifier 10.4230/LIPIcs...

Funding The authors were supported by the £3.5M EPSRC grant EP/R018472/1 (2018-2023)

1 Introduction: motivations, shape recognition problem and overview of results

Real-life objects are often represented by unstructured point clouds obtained by laser range scanning or by selecting salient or feature points in images [25]. Point clouds are easy to store and can be used as primitives for visualization [30]. The above advantages strongly motivate the problem of comparing and classifying unstructured point clouds.

Rigid objects are naturally studied up to rigid motion or isometry (including reflections), which is any map that preserves inter-point distances. The recognition of point clouds of the same number of points is practically solved by the histogram of all pairwise distances, which is a complete isometry invariant in general position [1].

Real shapes are often given in a distorted form because of noisy measurements, when points are perturbed, missed or accidentally added. One of the first approaches to recognize nearly identical point clouds A, B of different sizes in the same metric space, for example in \mathbb{R}^m , is to use the *Hausdorff* distance [16] $\text{HD}(A, B) = \min \epsilon \geq 0$ such that the first cloud A is covered by ϵ -balls centered at all points of B and vice versa.

However, we also need to take into account infinitely many potential isometries of the ambient space \mathbb{R}^m . The exact computation of $\inf_f \text{HD}(f(A), B)$ minimized over isometries f



© Yury Elkin, Vitaliy Kurlin;
licensed under Creative Commons License CC-BY
Leibniz International Proceedings in Informatics
LIPICS Schloss Dagstuhl – Leibniz-Zentrum für Informatik, Dagstuhl Publishing, Germany

of \mathbb{R}^m has a high polynomial complexity already for dimension $m = 2$ [6]. An approximate algorithm is cubic in the number of points for $m = 3$ [15].

This paper extends the 12-page conference version [11], which introduced the new invariant mergegram but didn't prove its continuity under perturbations. In addition to the proof of continuity, another contribution is Theorem 4.6 showing how to reconstruct a dendrogram of single-linkage clustering from a mergegram in general position.

The practical novelty is the harder recognition problem including perturbations of isometries within wider classes of affine and projective maps motivated by Computer Vision applications. Indeed different positions of cameras produce projectively equivalent images of the same rigid shape. The new experiments in section 6 extensively compared several approaches on 15000 clouds obtained from real images, see examples in Fig. 1.



■ **Figure 1** Example images from the dataset of mythical creatures, which was introduced in [2].

► **Problem 1.1** (isometry shape recognition under noise). Find an isometry invariant of point clouds in \mathbb{R}^m that is (a) independent of a cloud size, (b) provably continuous under perturbations of a cloud, (c) computable in a near linear time in the size of a cloud, and (d) more efficient for recognizing isometry classes of clouds than past invariants. ■

The key contributions are proofs of Theorems 4.6, 5.4 and Fig. 9, 10, 11 showing that the mergegram achieves a state-of-the-art recognition on substantially distorted images.

2 Related work on isometry shape recognition and Topological Data Analysis

For the isometry classification of clouds consisting of the same number of points, the easiest invariant is the distribution of all pairwise distances, whose completeness (or injectivity) was proved for all point clouds in general (non-singular) position in \mathbb{R}^m [1].

Fixed point clouds $A, B \subset \mathbb{R}^m$ of different sizes can be pairwise compared by the Hausdorff distance [16] $\text{HD}(A, B) = \max\{\sup_{p \in A} d_B(p), \sup_{q \in B} d_A(q)\}$, where $d_B(p) = \inf_{q \in B} d(p, q)$ is the (Euclidean or another) distance from a point $p \in A$ to the cloud B .

The rigid shape recognition problem for non-fixed clouds A, B is harder because of infinitely many potential isometries that can match A, B exactly or approximately. Partial cases of this problem were studied for clouds representing surfaces [10] and when two clouds have a given isometric matching of one pair of points [23]. Shape Google by Ovsjanikov et al. practically extends these ideas to non-rigid shape recognition [22].

The most general framework for the isometry shape recognition of point cloud data was proposed by Mémoi and Sapiro [20]. They studied the Gromov-Hausdorff distance $d_{GH}(A, B) = \inf_{f, g, M} \text{HD}(f(A), g(B))$ minimized over all isometric embeddings $f : A \rightarrow M$ and $g : B \rightarrow M$ of given point clouds into a metric space M . Since the above definitions involve even more minimizations over infinitely many maps and spaces, GH can be only

approximated. The Farthest Point Sampling (FPS) has a quadratic complexity in the number of points [20, section 3.6] and was successfully tested on small clouds.

The proposed invariant mergegram extends the 0-dimensional persistence in the area of Topological Data Analysis (TDA), which grew from the theory of size functions [28]. TDA views a point cloud $A \subset \mathbb{R}^m$ not by fixing any distance threshold but across all scales s , for example by blurring given points to balls of a variable radius s . The resulting evolution of topological shapes is summarized by a persistence diagram, which is invariant under isometries of \mathbb{R}^m . TDA can be combined with machine learning and statistical tools due to stability under noise, which was first proved by Cohen-Steiner et al. [9] and then extended to a very general form by Chazal et al. [5].

In dimension 0 the *persistence diagram* $\text{PD}(A)$ for distance-based filtrations of a point cloud A consists of the pairs $(0, s) \in \mathbb{R}^2$, where values of s are distance scales at which subsets of A merge by the single-linkage clustering. These scales equal half-lengths of edges in a *Minimum Spanning Tree* $\text{MST}(A)$. If distances between all points of A are known, $\text{MST}(A)$ is a connected graph with the vertex set A and a minimal total length.

Representing a point cloud A by $\text{PD}(A)$ loses a lot of geometry of A , but gains stability under perturbations, which can be expressed in the case of point clouds as $\text{BD}(\text{PD}(A), \text{PD}(B)) \leq \text{HD}(A, B)$. Here the *bottleneck distance* BD between diagrams is defined as a minimum $\epsilon \geq 0$ such that all pairs of $\text{PD}(A)$ can be bijectively matched to ϵ -close points of $\text{PD}(B)$ or to diagonal pairs (s, s) , and vice versa. Here ϵ -closeness of pairs (a, c) and (b, d) in \mathbb{R}^2 is measured in the distance $L_\infty = \max\{|a - b|, |c - d|\}$.

The *mergegram* extends $\text{PD}(A)$ to a stronger invariant whose stability under perturbations in the above sense is proved in section 5 for the first time. The idea of a mergegram is related to the Reeb graph [24] or the merge tree [21] for the sublevel set filtration of a scalar function. The mergegram MG is defined at a more abstract level for any clustering dendrogram, which can be reconstructed from MG in general position.

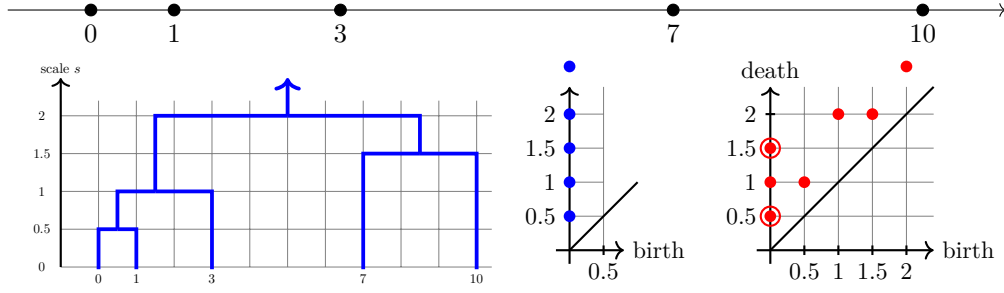
Since any persistence diagram and a mergegram are unordered collections of pairs, the experiments in section 6 will use the neural network *PersLay* [4] whose output is invariant under permutations of input points by design. *PersLay* extends the neural network *DeepSet* [29] for unordered sets and introduces new layers to specifically handle persistence diagrams, as well as a new form of representing such permutation-invariant layers. In other related work deep learning was recently applied to outputs of hierarchical clustering [13], [7], [17] and to 0-dimensional persistence [8], [14].

3 Single-linkage clustering and the invariant mergegram of a dendrogram

► **Example 3.1.** Fig. 2 illustrates the key concepts before formal Definitions 3.2, 3.4, 3.6 for the point cloud $A = \{0, 1, 3, 7, 10\}$ in the real line \mathbb{R} . Imagine that we gradually blur original data points by growing disks of the same radius s around the given points.

The disks of the closest points 0, 1 start overlapping at the scale $s = 0.5$ when these points merge into one cluster $\{0, 1\}$. This merger is shown by blue arcs joining at the node at $s = 0.5$ in the single-linkage dendrogram, see the bottom left picture in Fig. 2. The persistence diagram PD in the bottom middle picture of Fig. 2 represents this merger by the pair $(0, 0.5)$ meaning that a singleton cluster of (say) point 1 was born at the scale $s = 0$ and then died later at $s = 0.5$ by merging into another cluster of point 0.

XX:4 The mergegram of a dendrogram and its stability



■ **Figure 2** **Top:** the 5-point cloud $A = \{0, 1, 3, 7, 10\} \subset \mathbb{R}$. **Bottom** from left to right: single-linkage dendrogram $\Delta_{SL}(A)$ from Definition 3.2, the 0D persistence diagram PD from Definition 4.4 and the new mergegram MG from Definition 3.6, where double circles show pairs of multiplicity 2.

When clusters $\{0, 1, 3\}$ and $\{7, 10\}$ merge at $s = 2$, this event was previously encoded in the persistence diagram by the single pair $(0, 2)$ meaning that one cluster inherited from (say) point 7 was born at $s = 0$ and died at $s = 2$. The new mergegram in the bottom right picture of Fig. 2 represents the above merger by the following two pairs. The pair $(1, 2)$ means that the cluster $\{0, 1, 3\}$ is merging at the current scale $s = 2$ and was previously formed at the smaller scale $s = 1$. The pair $(1.5, 2)$ means that another cluster $\{7, 10\}$ is merging at the scale $s = 2$ and was previously formed at $s = 1.5$.

The 0D persistence diagram represents the cluster of the whole cloud A by the pair $(0, +\infty)$, because A was inherited from a singleton cluster starting from $s = 0$. The mergegram represents the same cluster A by the pair $(2, +\infty)$, because A was formed during the last merger of $\{0, 1, 3\}$ and $\{7, 10\}$ at $s = 2$ and continues to live as $s \rightarrow +\infty$.

In the above dendrogram every vertical arc going up from a scale b to d contributes one pair (b, d) to the mergegram. So both singleton clusters $\{7\}$, $\{10\}$ merging at $s = 1.5$ contribute one pair $(0, 1.5)$ of multiplicity two shown by two red circles in Fig. 2.

► **Definition 3.2** (single-linkage clustering). Let A be a finite set in a metric space X with a distance $d : X \times X \rightarrow [0, +\infty)$. Given a distance threshold, which will be called a scale s , any points $a, b \in A$ should belong to one *SL cluster* if and only if there is a finite sequence $a = a_1, \dots, a_m = b \in A$ such that any two successive points have a distance at most s , so $d(a_i, a_{i+1}) \leq s$ for $i = 1, \dots, m - 1$. Let $\Delta_{SL}(A; s)$ denote the collection of SL clusters at the scale s . For $s = 0$, any point $a \in A$ forms a singleton cluster $\{a\}$. Representing each cluster from $\Delta_{SL}(A; s)$ over all $s \geq 0$ by one point, we get the *single-linkage dendrogram* $\Delta_{SL}(A)$ visualizing how clusters merge, see the first bottom picture in Fig. 2. ■

For any $s > 0$, all SL clusters $\Delta_{SL}(A; s)$ can be obtained as connected components of a Minimum Spanning Tree $MST(A)$ by removing all edges longer than s .

► **Definition 3.3** (partition set $\mathbb{P}(A)$). For any set A , a *partition* of A is a finite collection of non-empty disjoint subsets $A_1, \dots, A_k \subset A$ whose union is A . The *single-block* partition of A consists of the set A itself. The *partition set* $\mathbb{P}(A)$ consists of all partitions of A . ■

The partition set $\mathbb{P}(A)$ of the abstract set $A = \{0, 1, 2\}$ consists of the five partitions

$$(\{0\}, \{1\}, \{2\}), \quad (\{0, 1\}, \{2\}), \quad (\{0, 2\}, \{1\}), \quad (\{1, 2\}, \{0\}), \quad (\{0, 1, 2\}).$$

For example, the collections $(\{0\}, \{1\})$ and $(\{0, 1\}, \{0, 2\})$ are not partitions of A .

Definition 3.4 below extends a dendrogram from [3, section 3.1] to arbitrary (possibly, infinite) sets A . Since every partition of A is finite by Definition 3.3, we don't need to add that an initial partition of A is finite. Non-singleton sets are now allowed.

► **Definition 3.4** (dendrogram Δ of merge sets). A *dendrogram* Δ over any set A is a function $\Delta : [0, +\infty) \rightarrow \mathbb{P}(A)$ of a scale $s \geq 0$ satisfying the following conditions.

(3.4a) There exists a scale $r \geq 0$ such that $\Delta(A; s)$ is the single block partition for $s \geq r$.

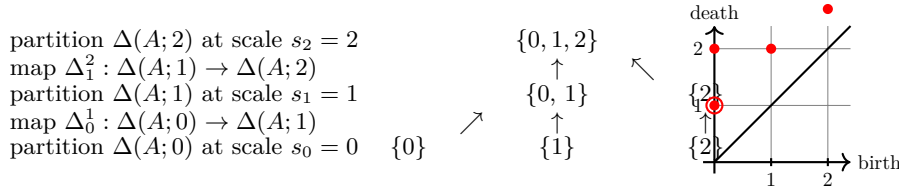
(3.4b) If $s \leq t$, then $\Delta(A; s)$ *refines* $\Delta(A; t)$, so any set from $\Delta(t)$ is a subset of some set from $\Delta(A; t)$. These inclusions of subsets of X induce the natural map $\Delta_s^t : \Delta(s) \rightarrow \Delta(t)$.

(3.4c) There are finitely many *merge scales* s_i such that

$$s_0 = 0 \text{ and } s_{i+1} = \sup\{s \mid \text{the map } \Delta_s^t \text{ is identity for } s' \in [s_i, s)\}, i = 0, \dots, m-1.$$

Since $\Delta(A; s_i) \rightarrow \Delta(A; s_{i+1})$ is not an identity map, there is a subset $B \in \Delta(s_{i+1})$ whose preimage consists of at least two subsets from $\Delta(s_i)$. This subset $B \subset X$ is called a *merge set* and its *birth* scale is s_i . All sets of $\Delta(A; 0)$ are merge sets at the birth scale 0. The *life*(B) is the interval $[s_i, t)$ from its birth scale s_i to its *death* scale $t = \sup\{s \mid \Delta_{s_i}^s(B) = B\}$. ■

Dendrograms are usually drawn as trees whose nodes represent all sets from the partitions $\Delta(A; s_i)$ at merge scales. Edges of such a tree connect any set $B \in \Delta(A; s_i)$ with its preimages under $\Delta(A; s_i) \rightarrow \Delta(A; s_{i+1})$. Fig. 3 shows Δ for $A = \{0, 1, 2\}$.



■ **Figure 3** The dendrogram Δ on $A = \{0, 1, 2\}$ and its mergegram $\text{MG}(\Delta)$ from Definition 3.6.

In Fig. 3 the partition $\Delta(A; 1)$ consists of $\{0, 1\}$ and $\{2\}$. The maps Δ_s^t induced by inclusions respect the compositions in the sense that $\Delta_s^t \circ \Delta_r^s = \Delta_r^t$ for any $r \leq s \leq t$. For example, $\Delta_0^1(\{0\}) = \{0, 1\} = \Delta_0^1(\{1\})$ and $\Delta_0^1(\{2\}) = \{2\}$, so Δ_0^1 is a well-defined map from the partition $\Delta(A; 0)$ of 3 singleton sets to $\Delta(A; 1)$, but isn't an identity.

At the scale $s_0 = 0$ the merge sets $\{0\}, \{1\}$ have life = $[0, 1)$, while the merge set $\{2\}$ has life = $[0, 2)$. At the scale $s_1 = 1$ the only merge set $\{0, 1\}$ has life = $[1, 2)$. At the scale $s_2 = 2$ the only merge set $\{0, 1, 2\}$ has life = $[2, +\infty)$. The notation Δ is motivated as the first (Greek) letter in the word dendrogram and by a Δ -shape of a typical tree.

Condition (3.4a) says that a partition of a set X is trivial for all large scales. Condition (3.4b) means that if the scale s is increasing, then sets from a partition $\Delta(s)$ can only merge but can not split. Condition (3.4c) implies that there are only finitely many mergers, when two or more subsets of X merge into a larger merge set.

► **Lemma 3.5.** [11, Lemma 3.3] Given a metric space (X, d) and a finite set $A \subset X$, the single-linkage dendrogram $\Delta_{SL}(X)$ from Definition 3.2 satisfies Definition 3.4. ■

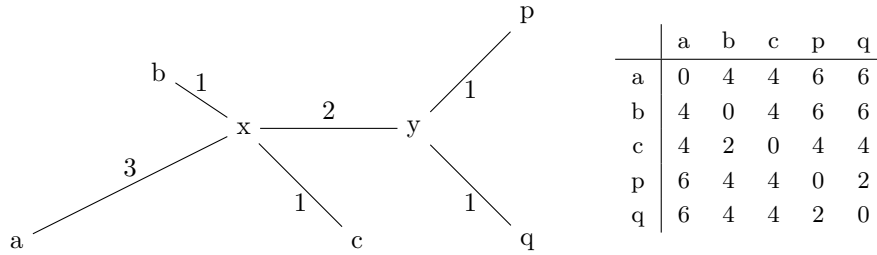
A *mergegram* represents life spans of merge sets by pairs (birth, death) $\in \mathbb{R}^2$.

XX:6 The mergegram of a dendrogram and its stability

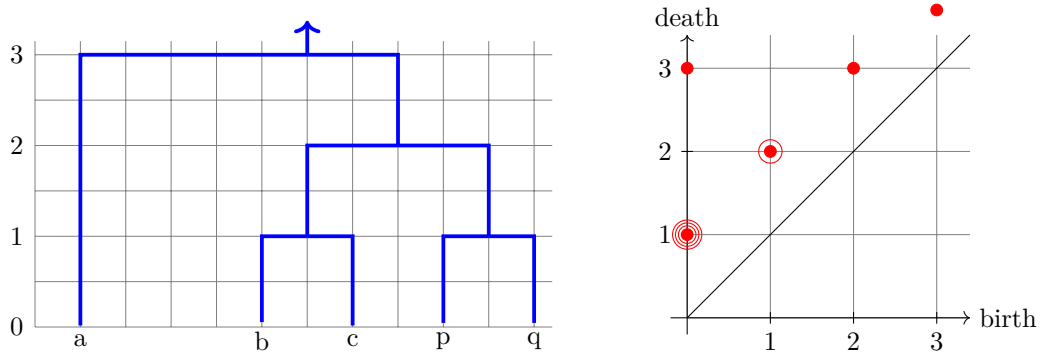
► **Definition 3.6** (mergegram $\text{MG}(\Delta)$). The *mergegram* of a dendrogram Δ has the pair $(\text{birth}, \text{death}) \in \mathbb{R}^2$ for each merge set B of Δ with $\text{life}(B) = [\text{birth}, \text{death}]$. If any life interval appears k times, the pair $(\text{birth}, \text{death})$ has the multiplicity k in $\text{MG}(\Delta)$. ■

If our input is a point cloud A in a metric space, then the mergegram $\text{MG}(\Delta_{SL}(A))$ is an isometry invariant of A , because $\Delta_{SL}(A)$ depends only on inter-point distances. Though $\Delta_{SL}(A)$ as any dendrogram is unstable under perturbations of points, the key advantage of $\text{MG}(\Delta_{SL}(A))$ is its stability, which will be proved in Theorem 5.8.

Fig. 4 shows the metric space $X = \{a, b, c, d, e\}$ with distances defined by the shortest path metric induced by the specified edge-lengths, see the distance matrix.



■ **Figure 4** The set $X = \{a, b, c, d, e\}$ has the distance matrix defined by the shortest path metric.



■ **Figure 5** Left: the dendrogram Δ for the single linkage clustering of the set 5-point set $X = \{a, b, c, d, e\}$ in Fig. 4. Right: the mergegram $\text{MG}(\Delta)$ with one pair $(0,1)$ of multiplicity 4.

The dendrogram Δ in the first picture of Fig. 5 generates the mergegram as follows:

- each of the singleton sets $\{b\}$, $\{c\}$, $\{p\}$, $\{q\}$ has pair $(0,1)$, so its multiplicity is 4;
- each of the merge sets $\{b, c\}$ and $\{p, q\}$ has the pair $(1,2)$, so its multiplicity is 2;
- the singleton set $\{a\}$ has the pair $(0,3)$; the merge set $\{b, c, p, q\}$ has the pair $(2,3)$;
- the full set $\{a, b, c, p, q\}$ continues to leave up to $s = 3$, hence has the pair $(3, +\infty)$.

4 Explicit relations between 0-dimensional persistence and mergegram

This section recalls the concept of persistence and then shows how any 0D persistence and dendrogram in general position can be reconstructed from a mergegram.

► **Definition 4.1** (persistence module \mathbb{V}). A *persistence module* \mathbb{V} over the real numbers \mathbb{R} is a family of vector spaces V_t , $t \in \mathbb{R}$ with linear maps $v_s^t : V_s \rightarrow V_t$, $s \leq t$ such that v_t^t is the identity map on V_t and the composition is respected: $v_s^t \circ v_r^s = v_r^t$ for any $r \leq s \leq t$. ■

The set of real numbers can be considered as a category \mathbb{R} in the following sense. The objects of \mathbb{R} are all real numbers. Any two real numbers such that $a \leq b$ define a single morphism $a \rightarrow b$. The composition of morphisms $a \rightarrow b$ and $b \rightarrow c$ is the morphism $a \rightarrow c$. In this language, a persistence module is a functor from \mathbb{R} to the category of vector spaces. A basic example of a persistence module \mathbb{V} is an interval module. An interval J between points $p < q$ in \mathbb{R} can be one of the following types: closed $[p, q]$, open (p, q) , half-open or half-closed $[p, q)$ and $(p, q]$, all encoded as follows:

$$[p^-, q^+] := [p, q], \quad [p^+, q^-] := (p, q), \quad [p^+, q^+] := (p, q], \quad [p^-, q^-] := [p, q).$$

The endpoints p, q can also take the infinite values $\pm\infty$, but without superscripts.

► **Example 4.2** (interval module $\mathbb{I}(J)$). For any interval $J \subset \mathbb{R}$, the *interval module* $\mathbb{I}(J)$ is the persistence module defined by the following vector spaces I_s and linear maps $i_s^t : I_s \rightarrow I_t$

$$I_s = \begin{cases} \mathbb{Z}_2, & \text{for } s \in J, \\ 0, & \text{otherwise;} \end{cases} \quad i_s^t = \begin{cases} \text{id}, & \text{for } s, t \in J, \\ 0, & \text{otherwise} \end{cases} \quad \text{for any } s \leq t.$$

The direct sum $\mathbb{W} = \mathbb{U} \oplus \mathbb{V}$ of persistence modules \mathbb{U}, \mathbb{V} is defined as the persistence module with the vector spaces $W_s = U_s \oplus V_s$ and linear maps $w_s^t = u_s^t \oplus v_s^t$.

We illustrate the abstract concepts above by geometric constructions. Let $f : X \rightarrow \mathbb{R}$ be a continuous function on a topological space. The *sublevel* sets $X_s^f = f^{-1}((-\infty, s])$ form nested subspaces $X_s^f \subset X_t^f$ for any $s \leq t$. The inclusions of the sublevel sets respect compositions similarly to a dendrogram Δ in Definition 3.4. On a metric space X with a metric $d : X \times X \rightarrow [0, +\infty)$, a typical example of a function $f : X \rightarrow \mathbb{R}$ is the distance d_A to a finite subset $A \subset X$. For any point $p \in X$, let $d_A(p)$ be the distance from p to a closest point of A . For any $r \geq 0$, the preimage $X_r^{d_A} = d_A^{-1}((-\infty, r]) = \{p \in X \mid d_A(p) \leq r\}$ is the union of closed balls with radius r and centers at all points $q \in A$. For example, $X_0^{d_A} = d_A^{-1}((-\infty, 0]) = A$ and $X_{+\infty}^{d_A} = d_A^{-1}(\mathbb{R}) = X$.

If we consider any continuous function $f : X \rightarrow \mathbb{R}$, we have the inclusion $X_s^f \subset X_r^f$ for any $s \leq r$. Hence all sublevel sets X_s^f form a nested sequence of subspaces within X . The above construction of a *filtration* $\{X_s^f\}$ can be considered as a functor from \mathbb{R} to the category of topological spaces. Below we discuss the simplest case of dimension 0.

► **Example 4.3** (persistent homology). For any topological space X , the 0-dimensional *homology* $H_0(X)$ is the vector space (with coefficients \mathbb{Z}_2) generated by all connected components of X . Let $\{X_s\}$ be any *filtration* of nested spaces, e.g. sublevel sets X_s^f based on a continuous function $f : X \rightarrow \mathbb{R}$. The inclusions $X_s \subset X_r$ for $s \leq r$ induce the linear maps between homology groups $H_0(X_s) \rightarrow H_0(X_r)$ and define the *persistent homology* $\{H_0(X_s)\}$, which satisfies the conditions of a persistence module from Definition 4.1. ■

If X is a finite set of m points, then $H_0(X)$ is the direct sum \mathbb{Z}_2^m of m copies of \mathbb{Z}_2 .

The persistence modules that can be decomposed as direct sums of interval modules can be described in a simple combinatorial way by persistence diagrams in \mathbb{R}^2 .

► **Definition 4.4** (persistence diagram $\text{PD}(\mathbb{V})$). Let a persistence module \mathbb{V} be decomposed as a direct sum of interval modules : $\mathbb{V} \cong \bigoplus_{l \in L} \mathbb{I}(p_l^*, q_l^*)$, where $*$ is $+$ or $-$. The *persistence diagram* $\text{PD}(\mathbb{V})$ is the multiset $\text{PD}(\mathbb{V}) = \{(p_l, q_l) \mid l \in L\} \setminus \{p = q\} \subset \mathbb{R}^2$. ■

The 0-dimensional persistence diagram of a topological space X with a continuous function $f : X \rightarrow \mathbb{R}$ is denoted by $\text{PD}\{H_0(X_s^f)\}$. Lemma 5.6 will prove that the merge module $M(\Delta)$ of any dendrogram Δ is decomposable into interval modules. Hence the mergegram $\text{MG}(\Delta)$ from can be interpreted as the persistence diagram of $M(\Delta)$.

The following result describes how the persistence diagram PD of the distance-based filtration of any point cloud A can be obtained from the mergegram $\text{MG}(\Delta_{\text{SL}}(S))$.

► **Theorem 4.5.** [11, Theorem 5.3] For a finite set A in a metric space (X, d) , let $d_A : X \rightarrow \mathbb{R}$ be the distance to A . Let the mergegram $\text{MG}(\Delta_{\text{SL}}(A))$ be a multiset $\{(b_i, d_i)\}_{i=1}^k$, where some pairs can be repeated. Then the persistence diagram $\text{PD}\{H_0(X_s^{d_A})\}$ is the difference of the multisets $\{(0, d_i)\}_{i=1}^k - \{(0, b_i)\}_{i=1}^k$ containing each pair $(0, s)$ exactly $\#b - \#d$ times, where $\#b$ is the number of births $b_i = s$ and $\#d$ is the number of deaths $d_i = s$. All trivial pairs $(0, 0)$ are ignored, alternatively we take $\{(0, d_i)\}_{i=1}^k$ only with $d_i > 0$. ■

Theorem 4.5 is illustrated by Example 3.1, where $A = \{0, 1, 3, 7, 10\}$ has the diagram $\text{PD}(A) = \{(0, 0.5), (0, 1), (0, 1.5), (0, 2), (0, +\infty)\}$ obtained from the mergegram

$$\text{MG}(\Delta_{\text{SL}}(A)) = \{(0, 0.5), (0, 0.5), (0, 1), (0, 1.5), (0, 1.5), (0.5, 1), (1, 2), (1.5, 2), (2, +\infty)\}$$

as follows: one pair $(0, 0.5) \in \text{PD}(A)$ comes from two deaths and one birth $s = 0.5$ in $\text{MG}(\Delta_{\text{SL}}(A))$. Similarly each of the pairs $(0, 1), (0, 1.5), (0, 2) \in \text{PD}(A)$ comes from two deaths and one birth equal to the same scale s . The cloud $B = \{0, 4, 6, 9, 10\} \subset \mathbb{R}$ in [11, Example 1.1] has exactly the same $\text{PD}(B) = \text{PD}(A)$ but different $\text{MG}(\Delta_{\text{SL}}(B)) \neq \text{MG}(\Delta_{\text{SL}}(A))$. This example together with Theorem 4.5 justify that the mergegram is strictly stronger than 0D persistence as an isometry invariant of a point cloud.

New Reconstruction Theorem 4.6 below can be contrasted with the weakness of 0D persistence $\text{PD}\{H_0(X_s^{d_A})\}$ consisting of only pairs $(0, s)$ whose finite deaths are half-lengths of edges in a Minimum Spanning Tree $\text{MST}(A)$. In Example 3.1 these scales $s = 0.5, 1, 1.5, 2$ are insufficient to reconstruct the SL dendrogram in Fig. 2. Such a unique reconstruction is possible by using the richer invariant mergegram as follows.

► **Theorem 4.6** (from a mergegram to a dendrogram). Let A be a finite point cloud in *general position* in the sense that all merge scales of A in a dendrogram Δ from Definition 3.4 are different. Then the dendrogram Δ can be reconstructed from its mergegram $\text{MG}(\Delta)$, uniquely up to a permutation of nodes in Δ at scale $s = 0$. ■

Proof. Consider all merge scales one by one in the increasing order starting from the smallest. The general position implies that only two clusters merge at any merge scale. For any current scale s , the mergegram contains exactly two pairs (b_1, s) and (b_2, s) .

For a smallest merge scale $s > 0$, the births should be $b_1 = b_2 = 0$. We start drawing a dendrogram Δ by merging any two points of A at this smallest scale s . To realize a merger at any larger s , we should select two clusters representing (b_1, s) and (b_2, s) .

If $b_i = 0$ then we take any of the unmerged points of A . If $b_i > 0$ then the already constructed dendrogram should contain a unique non-singleton cluster determined by the scale $b_i \in (0, s)$. Hence at any merge scale s we know how to select two clusters to merge. The only choice comes from choosing points of A or permuting notes of Δ . ◀

Following the above proof of Theorem 4.6 for the cloud $A = \{0, 1, 3, 7, 10\}$ in Example 3.1, the first two pairs $(0, 0.5) \in \text{MG}(\Delta_{\text{SL}}(A))$ indicate that we should merge two points of A at $s = 0.5$. The scale $s = 0.5$ uniquely determines this 2-point cluster.

The next two pairs $(0, 1), (0.5, 1)$ mean that the above cluster born at $s = 0.5$ should merge at $s = 1$ with a singleton cluster (any free point of A). The resulting 3-point cluster is uniquely determined by its merge scale $s = 1$. The further two pairs $(0, 1.5), (0.5, 1.5)$ say that a new 2-point cluster is formed at $s = 1.5$ by the two remaining points of A .

The final pairs $(1, 2), (1.5, 2)$ tell us to merge at $s = 2$ the two clusters formed earlier at $s = 1$ and $s = 1.5$. The resulting dendrogram Δ has the expected combinatorial structure as in Fig. 2, though we can draw Δ in another way by permuting points of A .

5 Stability of the mergegram for any single-linkage dendrogram

This section fully proves the stability of a mergegram, which was stated in [11, Theorem 7.4] without proving key Lemmas 5.6 and 5.7. For simplicity, we consider vector spaces with coefficients only in $\mathbb{Z}_2 = \{0, 1\}$, which can be replaced by any field.

Definition 5.1 introduces homomorphisms between persistence modules, which are needed to state the stability of persistence diagrams $\text{PD}\{H_0(X_s^f)\}$ under perturbations of a function $f : X \rightarrow \mathbb{R}$. This result will imply a stability for the mergegram $\text{MG}(\Delta_{\text{SL}}(A))$ for the dendrogram $\Delta_{\text{SL}}(A)$ of the single-linkage clustering of a set $A \subset X$.

► **Definition 5.1** (a homomorphism of a degree δ between persistence modules). Let \mathbb{U} and \mathbb{V} be persistent modules over \mathbb{R} . A *homomorphism* $\mathbb{U} \rightarrow \mathbb{V}$ of *degree* $\delta \in \mathbb{R}$ is a collection of linear maps $\phi_t : U_t \rightarrow V_{t+\delta}$, $t \in \mathbb{R}$, such that the diagram commutes for all $s \leq t$.

$$\begin{array}{ccc} U_s & \xrightarrow{u_s^t} & U_t \\ \phi_s \downarrow & & \downarrow \phi_t \\ V_{s+\delta} & \xrightarrow{v_{s+\delta}^{t+\delta}} & V_{t+\delta} \end{array}$$

Let $\text{Hom}^\delta(\mathbb{U}, \mathbb{V})$ be all homomorphisms $\mathbb{U} \rightarrow \mathbb{V}$ of degree δ . Persistence modules \mathbb{U}, \mathbb{V} are *isomorphic* if they have inverse homomorphisms $\mathbb{U} \rightarrow \mathbb{V} \rightarrow \mathbb{U}$ of degree 0. ■

For a persistence module \mathbb{V} with maps $v_s^t : V_s \rightarrow V_t$, the simplest example of a homomorphism of a degree $\delta \geq 0$ is $1_{\mathbb{V}}^\delta : \mathbb{V} \rightarrow \mathbb{V}$ defined by the maps $v_s^{s+\delta}$, $t \in \mathbb{R}$. So v_s^t defining the structure of \mathbb{V} shift all vector spaces V_s by the difference $\delta = t - s$.

The concept of interleaved modules below is an algebraic generalization of a geometric perturbation of a set X in terms of (the homology of) its sublevel sets X_s .

► **Definition 5.2** (interleaving distance ID). Persistence modules \mathbb{U} and \mathbb{V} are called δ -interleaved if there are homomorphisms $\phi \in \text{Hom}^\delta(\mathbb{U}, \mathbb{V})$ and $\psi \in \text{Hom}^\delta(\mathbb{V}, \mathbb{U})$ such that $\phi \circ \psi = 1_{\mathbb{V}}^{2\delta}$ and $\psi \circ \phi = 1_{\mathbb{U}}^{2\delta}$. The *interleaving distance* between the persistence modules \mathbb{U} and \mathbb{V} is $\text{ID}(\mathbb{U}, \mathbb{V}) = \inf\{\delta \geq 0 \mid \mathbb{U} \text{ and } \mathbb{V} \text{ are } \delta\text{-interleaved}\}$. ■

If $f, g : X \rightarrow \mathbb{R}$ are continuous functions such that $\|f - g\|_\infty \leq \delta$ in the L_∞ -distance, the modules $H_k\{f^{-1}(-\infty, s]\}$, $H_k\{g^{-1}(-\infty, s]\}$ are δ -interleaved for any k [9]. The last conclusion extends to persistence diagrams for the bottleneck distance below.

XX:10 The mergegram of a dendrogram and its stability

► **Definition 5.3** (bottleneck distance BD). Let multisets C, D contain finitely many points $(p, q) \in \mathbb{R}^2$, $p < q$, of finite multiplicity and all diagonal points $(p, p) \in \mathbb{R}^2$ of infinite multiplicity. For $\delta \geq 0$, a δ -matching is a bijection $h : C \rightarrow D$ such that $|h(a) - a|_\infty \leq \delta$ in the L_∞ -distance for any point $a \in C$. The *bottleneck distance* between persistence modules \mathbb{U}, \mathbb{V} is $\text{BD}(\mathbb{U}, \mathbb{V}) = \inf\{\delta \mid \text{there is a } \delta\text{-matching between } \text{PD}(\mathbb{U}), \text{PD}(\mathbb{V})\}$. ■

The original stability of persistence for sequences of sublevel sets was extended as Theorem 5.4 to q -tame persistence modules. A persistence module \mathbb{V} is q -tame if any non-diagonal square in the persistence diagram $\text{PD}(\mathbb{V})$ contains only finitely many of points, see [5, section 2.8]. Any finitely decomposable persistence module is q -tame.

► **Theorem 5.4** (stability of persistence modules). [5, isometry theorem 4.11] Let \mathbb{U} and \mathbb{V} be q -tame persistence modules. Then $\text{ID}(\mathbb{U}, \mathbb{V}) = \text{BD}(\text{PD}(\mathbb{U}), \text{PD}(\mathbb{V}))$, where ID is the interleaving distance, BD is the bottleneck distance between persistence modules. ■

► **Definition 5.5** (merge module $M(\Delta)$). For any dendrogram Δ on a finite set X , the *merge module* $M(\Delta)$ consists of the vector spaces $M_s(\Delta)$, $s \in \mathbb{R}$, and linear maps $m_s^t : M_s(\Delta) \rightarrow M_t(\Delta)$, $s \leq t$. For any $s \in \mathbb{R}$ and $A \in \Delta(s)$, the space $M_s(\Delta)$ has the generator or a basis vector $[A] \in M_s(\Delta)$. For $s < t$ and any set $A \in \Delta(s)$, if the image of A under Δ_s^t coincides with $A \subset X$, so $\Delta_s^t(A) = A$, then $m_s^t([A]) = [A]$, else $m_s^t([A]) = 0$. ■

scale $s_3 = +\infty$	0				0
map $m_2^{+\infty}$	\uparrow				\uparrow
scale $s_2 = 2$	\mathbb{Z}_2		0	0	$\{0, 1, 2\}$
map m_1^2	\uparrow		\uparrow	\uparrow	
scale $s_1 = 1$	$\mathbb{Z}_2 \oplus \mathbb{Z}_2$	0	0	$\{2\}$	$\{0, 1\}$
map m_0^1	\uparrow	\uparrow	\uparrow	\uparrow	
scale $s_0 = 0$	$\mathbb{Z}_2 \oplus \mathbb{Z}_2 \oplus \mathbb{Z}_2$	$\{0\}$	$\{1\}$	$\{2\}$	

■ **Figure 6** The merge module $M(\Delta)$ of the dendrogram Δ on the set $X = \{0, 1, 2\}$ in Fig. 3.

In a dendrogram Δ from Definition 3.4, any merge set A of Δ has $\text{life}(A) = [b, d]$ from its birth scale b to its death scale d . Lemmas 5.6 and 5.7 are proved for the first time.

► **Lemma 5.6** (merge module decomposition). For any dendrogram Δ from Definition 3.4, the merge module $M(\Delta) \cong \bigoplus_A \mathbb{I}(\text{life}(A))$ decomposes over all merge sets A . ■

Proof of Lemma 5.6. The goal is to prove that $M(\Delta) \cong \bigoplus_A \mathbb{I}(\text{life}(A))$. Recall that the interval module $\mathbb{I}(\text{life}(A))$ consists of only vector spaces 0 and \mathbb{Z}_2 . For a scale r , let $\mathbb{I}_r(\text{life}(A))$ be its vector space, whose generator is denoted by $[\mathbb{I}_r(\text{life}(A))]$. Define

$$\psi_r : M_r(\Delta) \rightarrow \bigoplus_A \mathbb{I}_r(\text{life}(A)) \text{ such that } [A] \rightarrow [\mathbb{I}_r(\text{life}(A))] \text{ for all } A \in \Delta(r),$$

$$\phi_r : \bigoplus_A \mathbb{I}_r(\text{life}(A)) \rightarrow M_r(\Delta) \text{ such that } [\mathbb{I}_r(\text{life}(A))] \rightarrow [A] \text{ for all } \text{life}(A) \text{ containing } r.$$

We will first prove that ϕ_r is well-defined. If $r \in \text{life}(A)$ then $A \in M_r(\Delta)$. We know that $M_r(\Delta)$ is generated by elements $A \in \Delta(r)$ for which $r \in \text{life}(A)$. Thus the compositions satisfy $\phi_r \circ \psi_r = \text{id}_r$ and $\psi_r \circ \phi_r = \text{id}_r$. It remains to prove that morphisms correctly behave under the functors ψ, ϕ . The proofs for both cases are essentially the same, thus we will prove it only for ψ . The goal is to prove that the following diagram commutes:

$$\begin{array}{ccc}
M_s(\Delta) & \xrightarrow{m_s^t} & M_t(\Delta) \\
\psi_s \downarrow & & \downarrow \psi_t \\
\bigoplus_A \mathbb{I}_s(\text{life}(A)) & \xrightarrow{i_s^t} & \bigoplus_A \mathbb{I}_t(\text{life}(A))
\end{array}$$

Here i_s^t is the direct sum of the corresponding maps of interval modules $\bigoplus_A (i_s^t)^A$. Let $[A]$ be an arbitrary generator of $M_r(\Delta)$. There are two possibilities how m_s^t can map $[A]$. If $t \in \text{life}(A)$, then $m_s^t([A]) = [A] \in M_t(\Delta)$ and by definition

$$\phi_t \circ m_s^t([A]) = [\mathbb{I}_t(\text{life}(A))].$$

Since both $s, t \in \text{life}(A)$, we also have that

$$m_s^t \circ \phi_t([A]) = [\mathbb{I}_t(\text{life}(A))] = \phi_t \circ m_s^t([A]).$$

Assume now that $t \notin \text{life}(A)$. Then $m_s^t([A]) = 0$ and thus $\phi_t(m_s^t([A])) = 0$. On the other hand $i_s^t \circ \phi_s([A]) = [\mathbb{I}_t(\text{life}(A))] = \mathbb{Z}_2$. Since $t \notin \text{life}(A)$, we get $i_s^t \circ \phi_s([A]) = 0$. ◀

► **Lemma 5.7** (merge modules interleaved). If subsets A, B of a metric space (X, d) have $\text{HD}(A, B) = \delta$, then the merge modules $M(\Delta_{SL}(A))$, $M(\Delta_{SL}(B))$ are δ -interleaved. ■

Proof of Lemma 5.7. The equality $\text{HD}(A, B) = \delta$ means that A is covered by the union of closed balls that have the radius δ and centers at all points $b \in B$. This union is the preimage is $d_B^{-1}([0, \delta])$, i.e. $A \subset d_B^{-1}([0, \delta])$. Extending the distance values by $s \geq 0$, we get $d_A^{-1}([0, s]) \subset d_B^{-1}([0, s + \delta])$ and similarly $d_B^{-1}([0, s]) \subset d_A^{-1}([0, s + \delta])$.

Let U be an arbitrary set in $\Delta_{SL}(A)$. Define map $\phi_r : M(A; r) \rightarrow M(B; r + \delta)$

$$\phi_r([U]) = \begin{cases} [U], & \text{if } r + \delta \in \text{life}(\Delta_{SL}(B), U), \\ 0, & \text{otherwise.} \end{cases}$$

Symmetrically for any $V \in \Delta_{SL}(B)$ we define $\psi_r : M(B; r) \rightarrow M(A; r + \delta)$

$$\psi_r([V]) = \begin{cases} [V], & \text{if } r + \delta \in \text{life}(\Delta_{SL}(A), V), \\ 0, & \text{otherwise.} \end{cases}$$

In the notation above, $\text{life}(\Delta_{SL}(B), U)$ is the $\text{life}(U)$ in the dendrogram $\Delta_{SL}(B)$. If $U \notin \Delta_{SL}(B)(t)$ for all values t , then $\text{life}(U) = \emptyset$. By symmetry it is enough to prove that the following diagrams commute:

$$\begin{array}{ccc}
M_s(\Delta_{SL}(A)) & \xrightarrow{m_s^t} & M_t(\Delta_{SL}(A)) \\
\phi_s \downarrow & & \downarrow \phi_t \\
M_{s+\delta}(\Delta_{SL}(B)) & \xrightarrow{m_{s+\delta}^{t+\delta}} & M_{t+\delta}(\Delta_{SL}(B))
\end{array}$$

$$\begin{array}{ccc}
& M_s(\Delta_{SL}(B)) & \\
\phi_{s-\delta} \nearrow & & \searrow \psi_s \\
M_{s-\delta}(\Delta_{SL}(A)) & \xrightarrow{m_{s-\delta}^{s+\delta}} & M_{s+\delta}(\Delta_{SL}(A))
\end{array}$$

XX:12 The mergegram of a dendrogram and its stability

We note first that if $[a, b] = (\text{life}(\Delta_{SL}(A), U), \text{life}(\Delta_{SL}(B), U))$, then $(\text{life}(\Delta_{SL}(B), U) \subseteq [a - \epsilon, b + \epsilon])$

We begin by proving commutativity of the first diagram. Let U be arbitrary element of $\Delta_{SL}(A)(s)$. If $t \notin \text{life}(\Delta_{SL}(A), U)$ then $\phi_t \circ m_s^t = 0$. If $s + \delta \notin \text{life}(\Delta_{SL}(B), U)$ or $t + \delta \notin \text{life}(\Delta_{SL}(B), U)$ then we are done. Since $t \notin \text{life}(\Delta_{SL}(A), U)$, it follows that $t + \delta \notin \text{life}(\Delta_{SL}(B), U)$. And thus with given assumptions the diagram commutes.

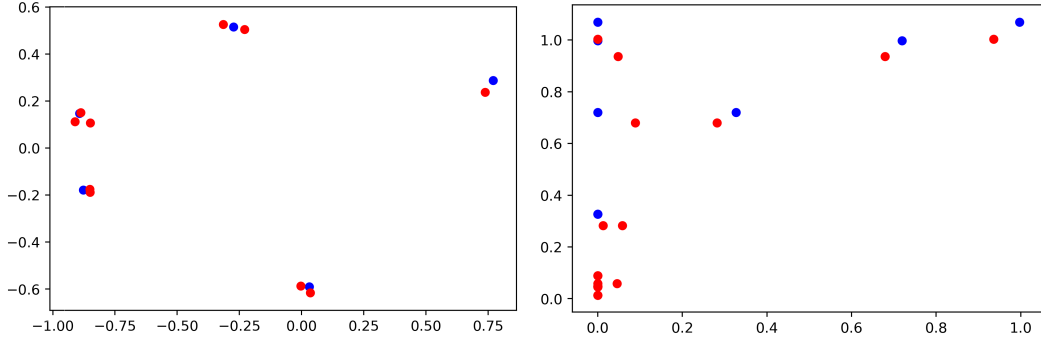
Assume now that $t + \delta \notin \text{life}(\Delta_{SL}(A), U)$. Then both $\phi_t(m_s^t(U)) = 0 = m_{s+\delta}^{t+\delta}(\phi_s(U))$. In the last case we assume that $t \in \text{life}(\Delta_{SL}(A), U)$ and $t + \delta \in \text{life}(\Delta_{SL}(B), U)$. In this case obviously $s + \delta \in \text{life}(\Delta_{SL}(B), U)$ and thus $\phi_t(m_s^t([U])) = [U] = m_{s+\delta}^{t+\delta}(\phi_s([U]))$.

For the second diagram assume now that $U \in M(\Delta_{SL}(A))(s - \delta)$. Assume first that $s \notin \text{life}(\Delta_{SL}(B), U)$, then $s + \delta \notin \text{life}(\Delta_{SL}(B), U)$ and $m_{s-\delta}^{s+\delta}([U]) = 0 = \psi_s(\phi_{s-\delta}[U])$.

Assume then that $s \in \text{life}(\Delta_{SL}(B), U)$. Now outcome of both maps ψ_s and $m_{s-\delta}^{s+\delta}$ depend on if $s + \delta \in \text{life}(\Delta_{SL}(A), U)$ and thus $m_{s-\delta}^{s+\delta}([U]) = \psi_s(\phi_{s-\delta}[U])$. Since all the diagrams commute, the required conclusion follows. ◀

► **Theorem 5.8 (stability of a mergegram).** The mergegrams of any finite point clouds A, B in a metric space (X, d) satisfy $\text{BD}(\text{MG}(\Delta_{SL}(A)), \text{MG}(\Delta_{SL}(B))) \leq \text{HD}(A, B)$. Hence any small perturbation of a cloud A in the Hausdorff distance yields a similarly small perturbation in the bottleneck distance for its mergegram $\text{MG}(\Delta_{SL}(A))$. ■

Proof. The given clouds $A, B \subset X$ with $\text{HD}(A, B) = \delta$ have δ -interleaved merge modules by Lemma 5.7, so $\text{ID}(\text{MG}(\Delta_{SL}(A)), \text{MG}(\Delta_{SL}(B))) \leq \delta$. Since any merge module $M(\Delta)$ is finitely decomposable, hence is q -tame by Lemma 5.6. The corresponding mergegram $\text{MG}(M(\Delta))$ satisfies Theorem 5.4, so $\text{BD}(\text{MG}(\Delta_{SL}(A)), \text{MG}(\Delta_{SL}(B))) \leq \delta$. ◀



■ **Figure 7 Left:** the cloud C of 5 blue points is close to the cloud C' of 10 red points in the Hausdorff distance. **Right:** the mergegrams are close in the bottleneck distance as predicted by Theorem 5.8.

Fig. 7 illustrates Theorem 5.8 on a cloud and its perturbation by showing their close mergegrams. The more extensive experiment on 100 clouds in [11, Fig. 8] similarly confirms that the mergegram is perturbed within expected bounds. The computational complexity of the mergegram $\text{MG}(\Delta_{SL}(A))$ was proved to be near linear in the number n of points in a cloud $A \subset \mathbb{R}^m$, see [11, Theorem 8.2]. The results above justify that the invariant mergegram satisfies conditions (a,b,c) of Isometry Recognition Problem 1.1.

6 New experiments on isometry recognition of substantially distorted real shapes

This section fulfills final condition (d) of Problem 1.1 by experimentally comparing the mergegram with 0D persistence and distributions of distances to neighbors on 15000 clouds. The earlier paper [11] did experiments only on randomly generated clouds.

We considered 15 classes of shapes represented by black and white images of mythical creatures [2], see Fig. 1. These shapes were chosen to make the shape recognition problem really challenging. Indeed, similar creatures from this dataset are represented by slightly different shapes, which can be hard to isometrically distinguish from each other. For example, several images of a horse include only minor differentiating features such as a saddle or a different tails, which makes horses nearly identical.

Shape generation. For each image, we generated 1000 perturbed images by affine and projective transformations to get 15000 distorted shapes split into 15 classes.

First we rotated each image around its central point by an angle generated uniformly in the interval $[0, 2\pi)$ using the function `cv::rotate` from the OpenCV library. If needed, we extended the resulting image to fit all black pixels of the rotated shape into a bounding box. Then both affine and projective transformations distort each image by using a noise parameter δ such that the value $\delta = 0$ represents the identity transformation.

Fig. 8 illustrates how an original image is randomly rotated, then randomly distorted by affine or projective transformations depending on the noise parameter δ .

Affine transformations are implemented as compositions of the already applied rotations above and the function `cv::resize()` from the OpenCV library. This function scales an image of size $w \times h$ by horizontal and vertical factors a, b sampled as follows.

- **Uniform noise:** $a \in [1 - \delta w, 1 + \delta w]$, $b \in [1 - \delta h, 1 + \delta h]$ have uniform distributions.
- **Gaussian noise:** $a \in \mathcal{N}(1, \delta h) \cap \mathbb{R}_+$ and $b \in \mathcal{N}(1, \delta w) \cap \mathbb{R}_+$ have Gaussian distributions with mean 1 and standard variance $\delta h, \delta w$, truncated to positive numbers.

Projective transformation are implemented as compositions of the already applied rotations above and the OpenCV function `cv::getPerspectiveTransform()` function, which is parametrized by 4-dimensional array $v = (a_0, a_1, a_2, a_3)$ consisting of points $a_i \in \mathbb{Z}^2$, $i = 0, 1, 2, 3$. This function maps the corners of the image as follows:

$$(0, 0) \mapsto a_0, (0, h) \mapsto a_1, (w, 0) \mapsto a_2 \text{ and } (w, h) \mapsto a_3.$$

Then the projective transformation of the rectangle $w \times h$ is uniquely determined by the above corners. The above points a_i are randomly sampled by using a noise parameter δ .

- **Uniform noise:** each coordinate has a uniform distribution with a noise parameter δ

$$a_0 \in [0, \delta w] \times [0, \delta h], \quad a_1 \in [0, \delta w] \times [h - \delta h, h],$$

$$a_2 \in [w - \delta w, w] \times [0, \delta h], \quad a_3 \in [w - \delta w, w] \times [h - \delta h, h].$$

- **Gaussian noise:** each coordinate has a Gaussian distribution truncated to the image

$$a_0 \in (\mathcal{N}(0, \delta w) \cap [0, w]) \times (\mathcal{N}(0, \delta h) \cap [0, h]),$$

$$a_1 \in (\mathcal{N}(0, \delta w) \cap [0, w]) \times (\mathcal{N}(h, \delta h) \cap [0, h]),$$

XX:14 The mergegram of a dendrogram and its stability

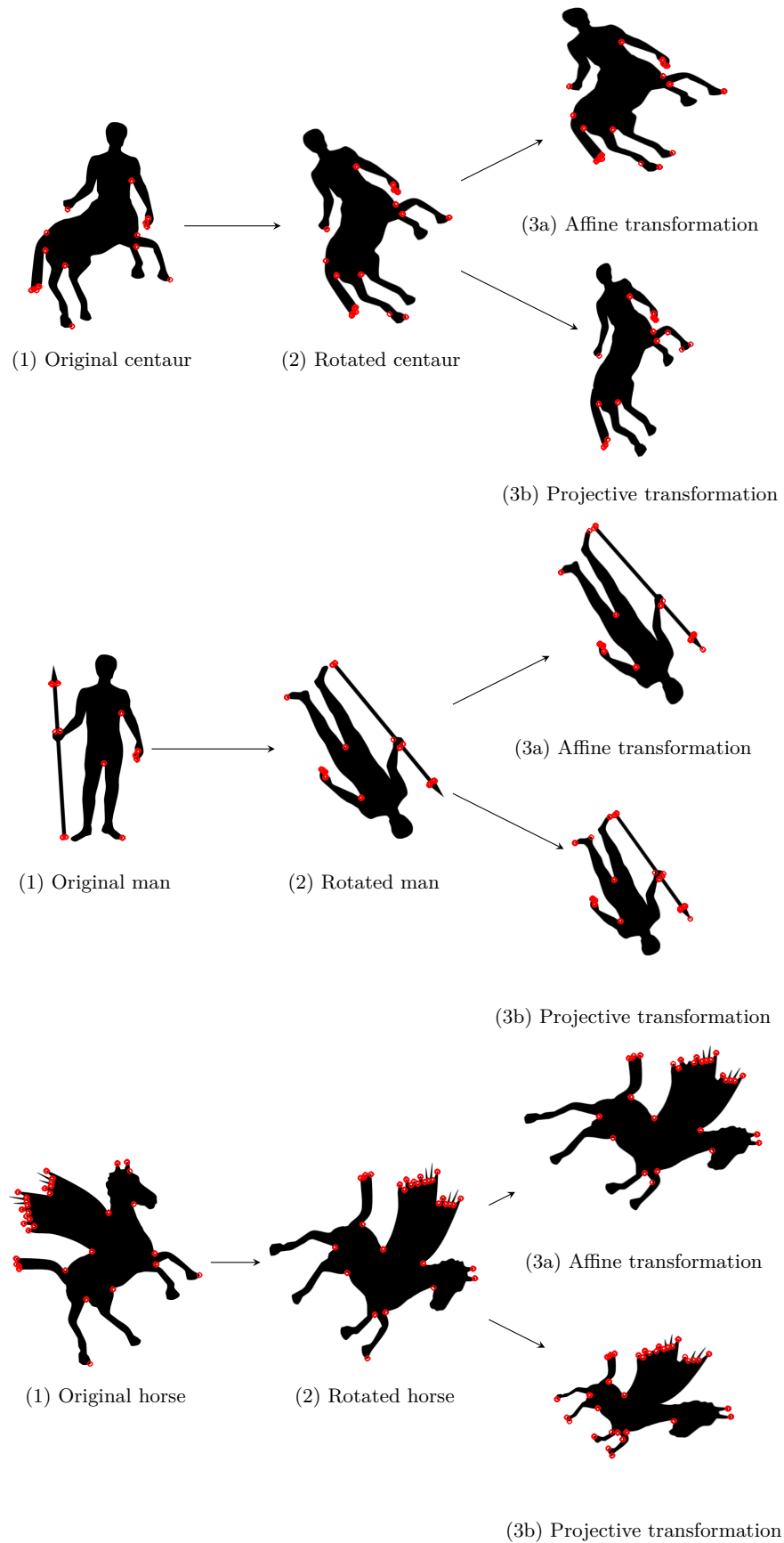


Figure 8 Generating distorted shapes by applying random rotations, affine and projective transformations, which substantially affect the extracted clouds of Harris corner points [27] in red.

$$a_2 \in (\mathcal{N}(w, \delta w) \cap [0, w]) \times (\mathcal{N}(0, \delta h) \cap [0, h]),$$

$$a_3 \in (\mathcal{N}(w, \delta w) \cap [0, w]) \times (\mathcal{N}(h, \delta h) \cap [0, h]).$$

Point cloud extraction. For each distorted image, we extract classical Harris point corners [27] due to their simplicity, see the red points in Fig. 8. For detecting corner points, the OpenCV function `cv::cornerHarris` was used with the parameters `blockSize = 3`, `apertureSize = 5`, `k = 0.04`, `thresh = 120`. However one can use any reliable algorithms such as FAST [26] or scale-invariant feature transform (SIFT) [19].

After describing the available point cloud data above, we specify condition (1.1d) of Isometry Recognition Problem 1.1 in the context of supervised machine learning.

► **Problem 6.1** (experimental recognition). Given a labeled dataset split into classes of similar but projectively distorted shapes, develop a supervised learning tool to recognize a class of distorted shapes with a high accuracy despite substantial noise.

Since all isometry invariants are independent of point ordering, the most suitable neural network is PersLay [4] whose output is invariant under permutations by design. Each layer is a combination of a coefficient layer $w(p) : \mathbb{R}^m \rightarrow \mathbb{R}$, a transformation $\phi(p) : \mathbb{R}^m \rightarrow \mathbb{R}^q$ and a permutation invariant layer op combined as follows

$$\text{PersLay}(D) = \text{op}(\{w(p)\phi(p)\}_{p \in D}), \text{ where } D \text{ is a diagram or multiset of points in } \mathbb{R}^m.$$

Coordinates of all input points are linearly normalized to $[0, 1]$. We have used the following parameters of the PersLay network for all experiments below.

The max layer $\text{MAX}(q)$ consists of the following functions.

- The coefficient layer $w : \mathbb{R}^m \rightarrow \mathbb{R}$ is the weight $w(x_1, \dots, x_m) = k|x_1 - x_2|$, where k is a trainable scalar and the dimension is typically $m = 2$.
- The transformation layer $\phi : \{\text{diagrams of points in } \mathbb{R}^m\} \rightarrow \mathbb{R}^q$ is the function $\phi(D) = \sum_{p \in D} \lambda p + \gamma \text{maxpool}(D) + \beta$, where λ, γ are $\mathbb{R}^{m \times q}$ trainable matrices, β is a \mathbb{R}^q trainable vector and maxpool returns a maximum value for every $i = 1, \dots, m$.
- The operational layer $\text{op} : \mathbb{R}^q \rightarrow \mathbb{R}^t$ puts all coordinates in increasing order and composes the result with standard densely connected layer [12] $\text{Dense} : \mathbb{R}^q \rightarrow \mathbb{R}^t$.

An output is a vector in \mathbb{R}^t for $t = 15$ of image classes. A final prediction is obtained by choosing a class with a largest coordinate in the output vector.

The image layer $\text{Im}[x, y]$ for integer parameters x, y and a multiset of points in the unit square $[0, 1]^2$ consists of the following functions.

- The coefficient layer $w : \mathbb{R}^2 \rightarrow \mathbb{R}$ is a piecewise constant function trained on $x \cdot y$ parameters, defined on the unit square partition

$$\mathcal{P}(x, y) = \left\{ \left[\frac{i}{x}, \frac{i+1}{x} \right] \times \left[\frac{j}{y}, \frac{j+1}{y} \right] \mid i = 0, \dots, x-1 \text{ and } j = 0, \dots, y-1 \right\}.$$

- Let $\phi_p : \mathbb{R}^2 \rightarrow \mathbb{R}$ be the Gaussian distribution centered at $p \in D$ with a trainable standard deviation σ . The transformation layer $\phi : \mathbb{R} \rightarrow \mathbb{R}^{xy}$ consists of xy functions ϕ_p , where p runs over all centroids of the partition $\mathcal{P}(x, y)$.
- The operation layer op takes the sum over the given point cloud. A final prediction is made by composing the operation layer with the Dense layer.

Finally, the PersLay network used the optimizer `tf.keras.adam` with the standard learning rate 0.01 and 150 epochs, the loss function `SparseCategoricalCrossEntropy`, the 80:20 of training and testing, a 5-fold Monte Carlo cross validation for each run.

Fig. 9, 10, 11 show that the mergegram MG consistently outperforms two other isometry invariants: 0D persistence and the multiset $NN(4)$ consisting of 4-tuple distances to neighbors per given point. The simpler multiset $NN(2)$ performed worse. A given cloud $C \subset \mathbb{R}^2$ was considered as a baseline input. The noise factors δ reached 25%, which means that original images were distorted up to a quarter of image sizes.

7 A discussion of novel contributions and further open problems

This paper has further demonstrated that the provably stable-under-noise invariant mergegram of a dendrogram is a fast and efficient tool in the challenging problem of isometry shape recognition, especially for substantially distorted images.

In comparison with the conference version [11], section 4 proved new Theorem 4.6 describing how to reconstruct a single-linkage dendrogram in general position from its much simpler mergegram. It is hard to define a continuous metric between dendrograms, especially because they can be unstable under perturbations. Theorem 4.6 allows us to measure a continuous similarity between dendrograms in general position as the bottleneck distance between their unique mergegrams. This distance can be computed in time $O(n^{1.5} \log n)$ [18] for diagrams consisting of at most n points.

Section 5 provided a full proof of stability of the mergegram under perturbations of points, while the earlier paper [11] only announced this result without proving highly non-trivial Lemmas 5.6 and 5.7, which required a heavy algebraic machinery.

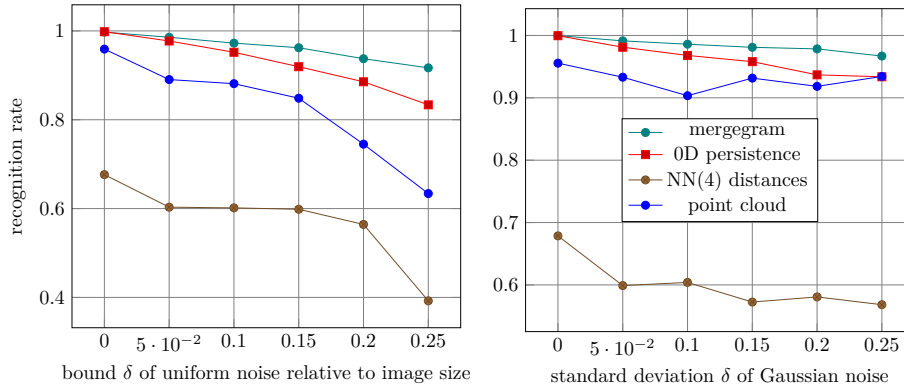
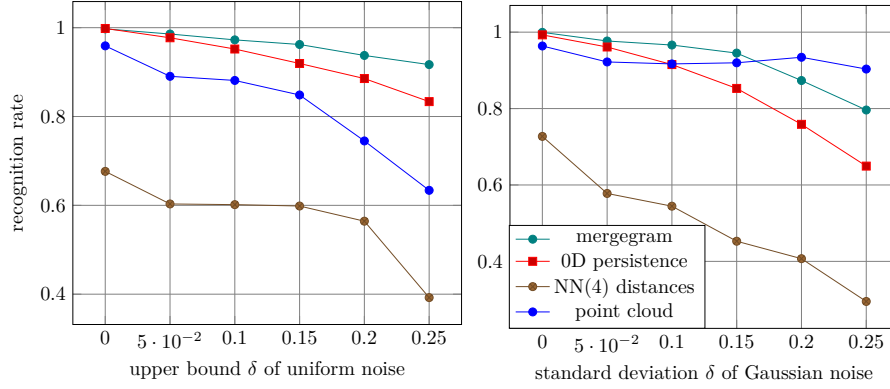
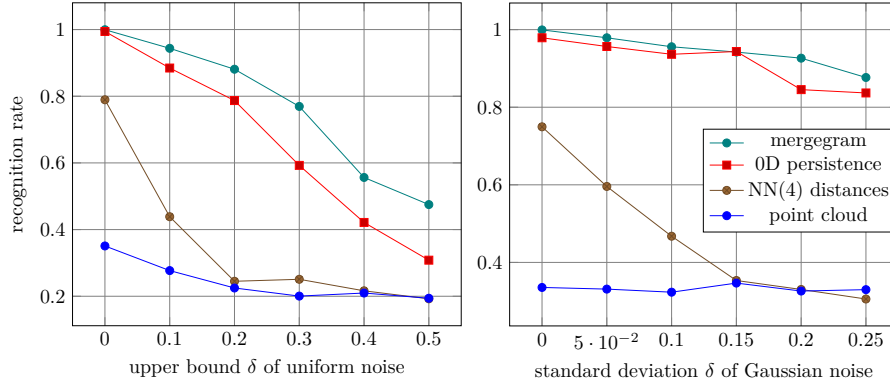


Figure 9 Recognition rates are obtained by training the max layer MAX(75) of PersLay on three isometry invariants and a cloud of corner points extracted from 15000 affinely distorted images.

Example 3.1 and the discussion following Theorem 4.5 justify that the invariant mergegram is strictly stronger than the 0D persistence. This theoretical fact is now confirmed by the new experiments on 15000 point clouds extracted from substantially distorted real shapes. In Fig. 9, 10, 11 the mergegram outperformed other isometry invariants. Since the distribution $NN(2)$ of distances to two closest neighbors per point performed badly, we have strengthened this invariant to $NN(4)$ of distances to four nearest neighbors. However, even $NN(4)$ performed always worse than the original point cloud, which can not be considered as an isometry invariant.



■ **Figure 10** Recognition rates are obtained by training the max layer MAX(75) of PersLay on isometry invariants and corner points extracted from 15000 projectively distorted images.



■ **Figure 11** Recognition rates are obtained by training the image layer IM[20,20] of PersLay on isometry invariants and a cloud of corner points extracted from 15000 affinely distorted images.

For very high levels of 20% and 25% distortions in projective transformations, the PersLay network trained on a point cloud achieved high recognition rates, because we have extensively tried many parameters in the layers MAX(75) and Im[20,20] for a best trade-off between accuracy and speed. The C++ code for the mergegram is at [11].

We thank all reviewers in advance for their valuable time and helpful suggestions.

References

- 1 Mireille Boutin and Gregor Kemper. On reconstructing n-point configurations from the distribution of distances or areas. *Advances in Applied Mathematics*, 32(4):709–735, 2004.
- 2 Alexander M Bronstein, Michael M Bronstein, Alfred M Bruckstein, and Ron Kimmel. Analysis of two-dimensional non-rigid shapes. *International Journal of Computer Vision*, 78(1):67–88, 2008.
- 3 Gunnar Carlsson and Facundo Memoli. Characterization, stability and convergence of hierarchical clustering methods. *Journal of machine learning research*, 11:1425–1470, 2010.
- 4 Mathieu Carriere, Frederic Chazal, Yuichi Ike, Theo Lacombe, Martin Royer, and Yuhei Umeda. Perslay: A neural network layer for persistence diagrams and new graph topological signatures. *AISTATS, arXiv:1904.09378*, 2020.
- 5 Frédéric Chazal, Vin De Silva, Marc Glisse, and Steve Oudot. *The structure and stability of persistence modules*. Springer, 2016.

XX:18 The mergegram of a dendrogram and its stability

- 6 Paul Chew, Michael Goodrich, Daniel Huttenlocher, Klara Kedem, Jon Kleinberg, and Dina Kravets. Geometric pattern matching under euclidean motion. *Computational Geometry*, 7:113–124, 1997.
- 7 Giansalvo Cirrincione, Gabriele Ciravegna, Pietro Barbiero, Vincenzo Randazzo, and Eros Pasero. The gh-exin neural network for hierarchical clustering. *Neural Networks*, 121:57–73, 2020.
- 8 James Clough, Nicholas Byrne, Ilkay Oksuz, Veronika A Zimmer, Julia A Schnabel, and Andrew King. A topological loss function for deep-learning based image segmentation using persistent homology. *IEEE Transactions on Pattern Analysis and Machine Intelligence*, 2020.
- 9 David Cohen-Steiner, Herbert Edelsbrunner, and John Harer. Stability of persistence diagrams. *Discrete & Computational Geometry*, 37(1):103–120, 2007.
- 10 Asi Elad and Ron Kimmel. Bending invariant representations for surfaces. In *Proceedings of Computer Vision and Pattern Recognition*, 2001.
- 11 Y. Elkin and V. Kurlin. The mergegram of a dendrogram and its stability. In *Proceedings of MFCS (Mathematical Foundations of Computer Science)*, 2020. URL: <https://github.com/YuryUoL/Mergegram>, doi:10.4230/LIPIcs.MFCS.2020.32.
- 12 Martín Abadi et al. TensorFlow: Large-scale machine learning on heterogeneous systems, 2015. URL: https://www.tensorflow.org/api_docs/python/tf/keras/layers/Dense, doi:10.5281/zenodo.4724125.
- 13 Guoji Fu, Chengbin Hou, and Xin Yao. Learning topological representation for networks via hierarchical sampling. In *International Joint Conference on Neural Networks (IJCNN)*, pages 1–8, 2019.
- 14 Rickard Brüel Gabriëlsson, Bradley J Nelson, Anjan Dwaraknath, and Primož Skraba. A topology layer for machine learning. In *International Conference on Artificial Intelligence and Statistics*, pages 1553–1563. PMLR, 2020.
- 15 Michael T Goodrich, Joseph SB Mitchell, and Mark W Orletsky. Approximate geometric pattern matching under rigid motions. *Trans. on Pattern Analysis and Machine Intelligence*, 21(4):371–379, 1999.
- 16 Daniel P Huttenlocher, Gregory A. Klanderman, and William J Rucklidge. Comparing images using the hausdorff distance. *Transactions on pattern analysis and machine intelligence*, 15(9):850–863, 1993.
- 17 Md Rezaul Karim, Oya Beyan, Achille Zappa, Ivan G Costa, Dietrich Rebholz-Schuhmann, Michael Cochez, and Stefan Decker. Deep learning-based clustering approaches for bioinformatics. *Briefings in bioinformatics*, 22(1):393–415, 2021.
- 18 Michael Kerber, Dmitriy Morozov, and Arnur Nigmatov. Geometry helps to compare persistence diagrams. In *Proceedings of ALLENEX*, pages 103–112, 2016.
- 19 David G Lowe. Object recognition from local scale-invariant features. In *Proceedings of the seventh IEEE international conference on computer vision*, volume 2, pages 1150–1157. Ieee, 1999.
- 20 Facundo Mémoli and Guillermo Sapiro. A theoretical and computational framework for isometry invariant recognition of point cloud data. *Foundations of Computational Mathematics*, 5(3):313–347, 2005.
- 21 Dmitriy Morozov, Kenes Beketayev, and Gunther Weber. Interleaving distance between merge trees. *Discrete and Computational Geometry*, 49(22-45):52, 2013.
- 22 Maks Ovsjanikov, Alexander M Bronstein, Michael M Bronstein, and Leonidas J Guibas. Shape google: a computer vision approach to isometry invariant shape retrieval. In *International Conference on Computer Vision workshops*, pages 320–327, 2009.
- 23 Maks Ovsjanikov, Quentin Mérigot, Facundo Mémoli, and Leonidas Guibas. One point isometric matching with the heat kernel. In *Computer Graphics Forum*, volume 29, pages 1555–1564, 2010.
- 24 Salman Parsa. A deterministic $O(m \log m)$ time algorithm for the reeb graph. *Discrete & Computational Geometry*, 49(4):864–878, 2013.

- 25 Mark Pauly, Markus Gross, and Leif P Kobbelt. Efficient simplification of point-sampled surfaces. In *IEEE Visualization*, pages 163–170, 2002.
- 26 Edward Rosten, Reid Porter, and Tom Drummond. Faster and better: A machine learning approach to corner detection. *IEEE transactions on pattern analysis and machine intelligence*, 32(1):105–119, 2008.
- 27 Javier Sánchez, Nelson Monzón, and Agustín Salgado De La Nuez. An analysis and implementation of the harris corner detector. *Image Processing On Line*, 2018.
- 28 Alessandro Verri, Claudio Uras, Patrizio Frosini, and Massimo Ferri. On the use of size functions for shape analysis. *Biological cybernetics*, 70(2):99–107, 1993.
- 29 Manzil Zaheer, Satwik Kottur, Siamak Ravanbakhsh, Barnabas Poczos, Russ R Salakhutdinov, and Alexander J Smola. Deep sets. In *Advances in neural information processing systems*, pages 3391–3401, 2017.
- 30 Matthias Zwicker, Mark Pauly, Oliver Knoll, and Markus Gross. Pointshop 3d: An interactive system for point-based surface editing. *ACM Transactions on Graphics (TOG)*, 21(3):322–329, 2002.